Alignment of Tellurium Nanorods *via* a Magnetization–Alignment–Demagnetization ("MAD") Process Assisted by an External Magnetic Field

Jiayin Yuan,[†] Haitao Gao,[‡] Felix Schacher,[†] Youyong Xu,[†] Reinhard Richter,[§] Wolfgang Tremel,[‡] and Axel H. E. Müller[†,*]

[†]Makromolekulare Chemie II, Universität Bayreuth, D-95440 Bayreuth, Germany, [‡]Institut für Anorganische Chemie und Analytische Chemie, Johannes Gutenberg-Universität Mainz, D-55099 Mainz, Germany, and [§]Experimentalphysik V, Universität Bayreuth, D-95440 Bayreuth, Germany

ABSTRACT Tellurium (Te) nanorods have been successfully aligned on a solid substrate *via* a magnetization–alignment–demagnetization ("MAD") process in the presence of an external magnetic field. Te nanorods carrying a poly(*tert*-butyl methacrylate) shell were first converted into magnetic nanocylinders by assembling magnetite nanoparticles on their surface *via* a hydrophobic interaction in THF. We demonstrate that, below a critical concentration of the nanoparticles, this assembly process is able to quantitatively tune the magnetite nanoparticles' density on the nanorods in terms of their stoichiometric ratio. Due to the polymer and surfactant on their surface, the formed magnetic nanocylinders are soluble in THF and aligned when dried on a solid substrate in the presence of an external magnetic field. The demagnetization of the prealigned nanocylinders was achieved *via* an acid-etching process, leaving Te nanorods in an aligned state. This MAD process can be extended as a general procedure for other nonmagnetic 1-D nanostructures. Additionally, the nonetched magnetic nanocylinders can be potentially applied in field of magnetorheology.

KEYWORDS: tellurium nanorods · magnetite nanoparticles · magnetic nanocylinders · alignment · assembly

There has been expanding interest in one-dimensional (1-D) nanostructures in the past decade, such as nanorods, nanotubes, or nanowires, due to a range of size- and geometry-dependent properties[1–4] and potential applications in optical and electronic devices,[5–7] sensing and imaging,[8,9] drug and gene delivery,[10,11] *etc*. So far, great progress has been achieved in developing numerous 1-D nanostructures through various techniques and methods.[12–17] Currently, the organization and manipulation of these 1-D nanostructures have attracted a lot of attention, as further scientific and technological advances in the application of 1-D nanostructures in functional nanodevices depend strongly on the ability to assemble them into ordered and complex architectures. It has been reported that the collective behavior and interparticle coupling in well-organized 1-D nanostructures resulted in new functions or significant improvement of their optoelectronic properties. For example, Alivisatos *et al.* demonstrated the formation of liquid crystal originating from the CdSe nanorod assembly;[18] Wang *et al.* showed that a nanowire nanogenerator, fabricated from vertically aligned ZnO nanowire arrays, produced continuous and stable direct-current output;[2] in another study, a polymer matrix containing aligned multiwalled carbon nanotubes exhibited improved and anisotropic mechanical properties.[19] To date, several techniques have allowed the spatial organization of 1-D nanostructures, including the use of bound ligands to stabilize anisotropic nanoparticles,[20–23] biorecognition,[24] template-directed self-assembly,[25–27] external electric or magnetic field introduced alignment,[28–31] interactions between segmented polymer–metal rods in selective solvents,[32] orientation-controlled growth on a substrate,[2,33] fluidic approach,[34] Langmuir–Blodgett technique,[35] mechanical straining of 1-D nanostructures in a polymer matrix,[36] liquid crystalline assisted approach,[37] and others.[38,39] Among them, external electric or magnetic field introduced alignment represents a noncontact, large-scale, low-cost, and easy-to-implement strategy. In the presence of an external electric field, carbon nanotubes as well as metallic nanowires have been fabricated into ordered structures.[40,41] In an external magnetic field, metallic (*i.e.*, nickel, cobalt, permalloys) ferromagnetic nanowires,[30,31,42,43] carbon nanotubes and nanofibers,[44,45] and nickel end-capped ZnO or copper–tin nanowires[46,47] have been successfully

*Address correspondence to axel.mueller@uni-bayreuth.de.

Received for review March 18, 2009 and accepted May 20, 2009.

Published online June 1, 2009.
10.1021/nn9002715 CCC: $40.75

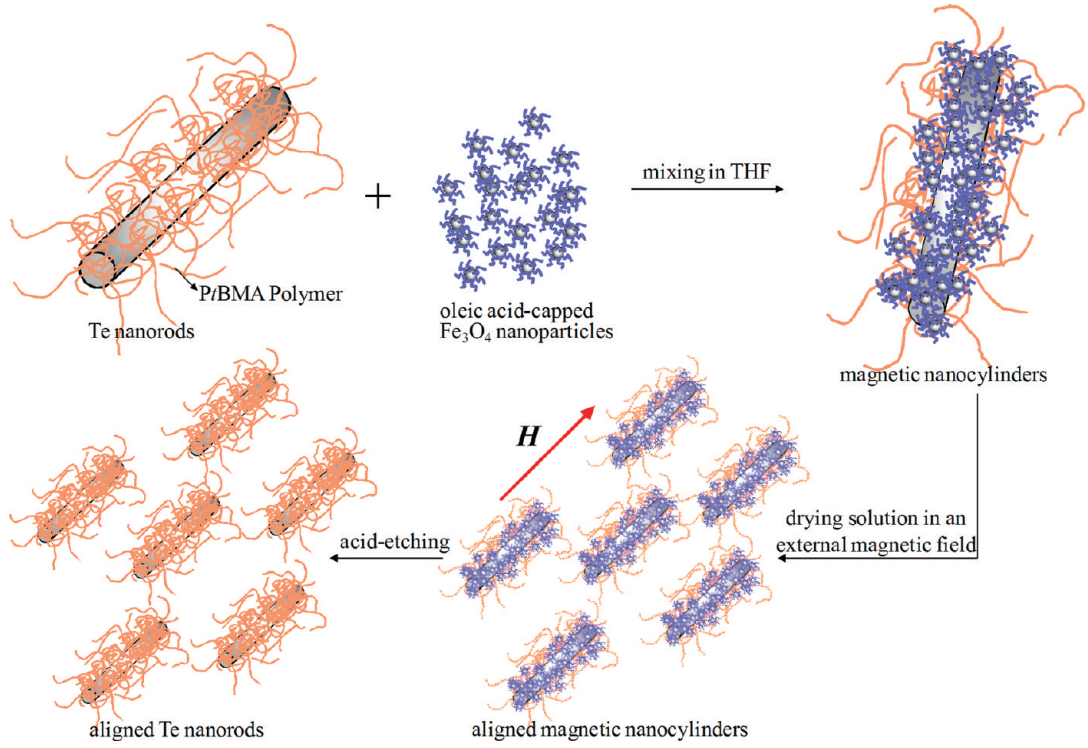

Scheme 1. Illustration of the alignment of Te nanorods *via* a MAD process assisted by an external magnetic field.

aligned. Recently, the manipulation of nonmagnetic Au−Ag nanorods by a magnetic field has been reported inside a ferrofluid.[48,49]

Very recently, we observed that tellurium (Te) nanorods covered by a layer of poly(*tert*-butyl methacrylate) (P*t*BMA) could assemble inorganic (Te or magnetite) nanoparticles onto their surface *via* a hydrophobic interaction.[50] This interesting finding leads to continuing research on the Te nanorods functionalized with magnetite nanoparticles, named magnetic nanocylinders, which combine the uniform geometry of the Te nanorods and the magnetic function of the magnetite nanoparticles. In this paper, we report a facile and unique process, named magnetization−alignment−demagnetization ("MAD") process, to align Te nanorods parallel to an external magnetic field on a solid substrate, as illustrated in Scheme 1. In this process, we demonstrate for the first time the quantitative control of magnetite nanoparticles' density on the nanorods, supported by mathematic calculations, the aligning behavior of the formed magnetic nanocylinders, and the stepwise etching of prealigned magnetic nanocylinders into Te nanorods. In fact, to the best of our knowledge, this is the first example of a general approach to align nonmagnetic nanorods on a substrate in a magnetic field by decorating their surface with magnetite nanoparticles followed by selective removal of these nanoparticles.

Magnetic nanoparticles have been extensively studied due to their promising applications in the fields of magnetic fluids, catalysis, biotechnology/biomedicine, magnetic resonance imaging, data storage, and environmental remediation.[51] Among various magnetic nanomaterials, 1-D nanostructures have been the constant pursuit of researchers due to their unique utilizations as sensors, magnetic recording, and spintronic devices.[52−57] Template-assisted synthesis is the most frequently employed method;[30,31,33,42,43,52] magnetic−dipolar interaction-induced self-assembly,[53] sol−gel process,[54] and other methods[55] have also been used to prepare magnetic 1-D nanostructures. Here, as a coexistent advantage of the versatile MAD process, magnetic nanocylinders are constructed more easily compared to other synthetic methodologies. The advantages include the following: (1) No purification or post-treatment is required after mixing the nanoparticles and nanorods in THF. In our strategy, all particles are attached to the nanorods statistically below a critical concentration, leaving magnetic nanocylinders as the only pure product in solution. Although the coating of gold nanorods or carbon nanofibers with magnetic nanoparticles has been reported,[45,58] excessive reactants, byproducts, or free nanoparticles remained mixed with the resulting 1-D magnetic nanostructures. (2) The magnetic property of nanocylinders is quantitatively tunable by varying the stoichiometric ratio of these two components. We managed to control the population (from 17 to 597) of nanoparticles on individual nanorods in our approach. Magnetic properties, such as the magnetic moment of each nanocylinder, are proportional to the number of nanoparticles on it.[45] One can achieve a desired magnetic moment of the nanocylinders *via* a suitable stoichiometric ratio of nanoparticles to nanorods. (3) The size and aspect ratio of the magnetic nanocylinders stem from the Te

nanorods, which can be effectively controlled by changing the reactant concentration, the reaction media, purging time of the H_2Te gas, the type of polymers, *etc.*[50] (4) Due to the protective polymer and surfactant layer on their surface, these nanocylinders are well-dispersed in organic solvents, which facilitates the further processing. The unique coexistence of these four aspects represents the key advantage of our system over prior approaches.

RESULTS AND DISCUSSION

Synthesis and Characterization of Magnetite Nanoparticles and Te Nanorods. As the basic components to build the magnetic nanocylinders, magnetite nanoparticles and Te nanorods were separately prepared first. Figure 1A shows a representative transmission electron microscopy (TEM) image of the magnetite nanoparticles produced through the conventional co-precipitation method.[59,60] Since the nanoparticles are capped with oleic acid molecules and possess an alkyl layer on the surface, they are soluble in most organic solvents, such as cyclohexane, benzene, and also THF. The crystallinity of the nanoparticles was checked by high-resolution TEM (Figure 1B). There is clear evidence of lattice planes corresponding to the (220) planes of magnetite with 0.2967 nm interplanar spacing. Their size distribution histogram in Figure 1C, which resembles a Gaussian curve, shows that the nanoparticles studied in this article are on average 9.6 nm in diameter with a standard deviation of 21%. Electron diffraction measured from a large zone (Figure 1D) presents the distinct rings that can be indexed to the magnetite structure. The Mössbauer spectrum (see Supporting Information) further confirms the phase to be magnetite Fe_3O_4, which is typical for the magnetic nanoparticles obtained through the co-precipitation method.[61,62]

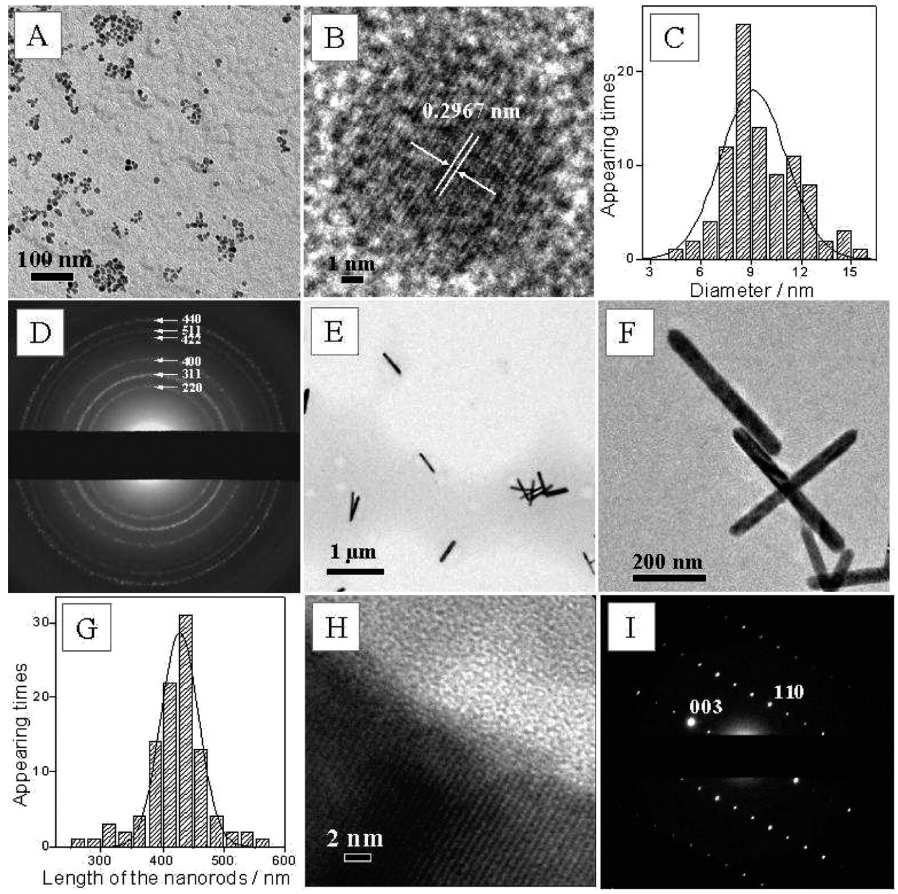

Figure 1. (A) TEM image of the as-synthesized magnetite nanoparticles; (B) high-resolution TEM image of a single nanoparticle; (C) size distribution histogram of the nanoparticles (black curve is the Gaussian fit); (D) selected area electron diffraction pattern of the nanoparticles; (E) TEM image of the Te (1) nanorods; (F) their enlarged view; (G) their length distribution histogram (black curve is the Gaussian fit); (H) high-resolution TEM image of a single nanorod; and (I) its corresponding electron diffraction pattern.

The Te nanorods were prepared by purging *in situ* generated H_2Te gas into a P*t*BMA polymer solution in THF at room temperature, as we reported earlier.[50] In this research, three types of Te nanorods with different aspect ratios were synthesized for the study of the magnetic nanocylinders. Their dimensions are listed in Table 1. As an example, a typical TEM image of the Te (1) nanorods is shown in Figure 1E. Due to the P*t*BMA polymer attached to the surface, the nanorods are very soluble and form a clear blue solution in THF. The TEM image in Figure 1F with a higher magnification exhibits the smooth surface of the nanorods. These nanorods are on average 422 ± 48 nm long and 47 ± 11 nm in diameter, giving an aspect ratio of 9. The length distribution histogram is present in Figure 1G, which matches a Gaussian distribution as well. The high-resolution TEM (Figure 1H) and its electron diffraction pattern (Figure 1I) prove that the Te nanorod is structurally single crystalline along the longitudinal axis (*c* axis), corresponding to the interplanar spacing between the (001) planes of the hexagonal lattice. Electron diffraction analysis of different single nanorods at varying tilting angles excludes the twinned crystal structure. From the above characterizations, both nanoparticles and nanorods as the constructing units are single crystalline with a nar-

TABLE 1. Three Types of Te Nanorods with Different Lengths and Diameters Obtained *via* TEM Investigation

sample	length/nm	diameter/nm	aspect ratio
Te (1)	422 ± 48	47 ± 11	9
Te (2)	295 ± 47	21 ± 5	14
Te (3)	473 ± 46	155 ± 32	3

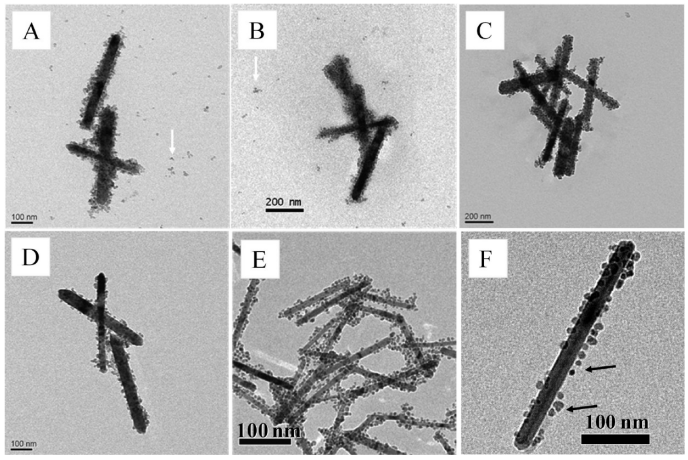

Figure 2. (A−D) Magnetic Te (1) nanocylinders prepared from Te (1) nanorods (60 mg/L) and different concentrations of magnetite nanoparticles: (A) 50.6 mg/L, (B) 16.8 mg/L, (C) 5.2 mg/L, and (D) 1.87 mg/L in THF. The stoichiometric ratios (nanoparticles to nanorods) are (A) 1625, (B) 539, (C) 167, and (D) 60 respectively. (E) Magnetic Te (2) nanocylinders prepared from Te (2) nanorods (33.7 mg/L) and magnetite nanoparticles (8.65 mg/L) with a stoichiometric ratio of 69. (F) Single Te (2) magnetic nanocylinder with *ca.* 50 nanoparticles.

row size distribution in their dimension and are soluble in THF.

Controlled Assembly of Magnetite Nanoparticles on Te Nanorods. The magnetic nanocylinders were produced by mixing the Te nanorod solution and magnetite nanoparticle solution in THF under strong mechanical shaking. During this process, the magnetite nanoparticles assembled onto the nanorod surface *via* the hydrophobic interaction[63] between the P*t*BMA layer on the nanorods and the alkyl chains on the nanoparticles. Figure 2A−D shows various TEM images of the magnetic Te (1) nanocylinders that were prepared with constant Te (1) nanorod concentration (60 mg/L) and decreasing concentration of nanoparticles from 50.6 mg/L (Figure 2A) to 1.87 mg/L (Figure 2D) in THF solution. All TEM images reveal that the nanoparticles tend to adhere onto the nanorod rather than stay in THF. By carefully examining the TEM images, the free nanoparticles, indicated by a white arrow, become evidently less and less from Figure 2A to Figure 2B until totally vanishing in Figure 2C,D. Due to the large gap between the nanoparticle concentrations in Figure 2B,C, an additional sample was prepared in the same way with only 6.5 mg/L of magnetite nanoparticles in THF solution, which showed the existence of free nanoparticles in the TEM investigation. Thus we define the concentration of the magnetite nanoparticles in Figure 2C (5.2 mg/L) as the critical concentration. Above it (Figure 2A,B), free nanoparticles exist in the THF solution; in contrast, below it, all nanoparticles will sit on the nanorods (Figure 2C,D), which leads to pure magnetic nanocylinders in THF.

A close view of the magnetic nanocylinders in Figure 2C,D indicates a statistical distribution of the nanoparticles on all Te nanorods. Since a triple amount of magnetite nanoparticles was introduced in Figure 2C compared to Figure 2D, the magnetic nanocylinders in Figure 2C have a higher density of nanoparticles. A calculation based on the concentrations of Te nanorods and Fe_3O_4 nanoparticles proves that each nanocylinder in Figure 2C carries *ca.* 167 nanoparticles and in Figure 2D only 60 (see Supporting Information). As the magnetic cylinders are based on the nanoparticles, their magnetic properties can be quantitatively tuned by loading different amounts of nanoparticles below the critical concentration. In the same manner, the critical concentration of the nanoparticles on Te (2) nanorods (33.7 mg/L) was determined to be 8.65 mg/L. The corresponding TEM image is shown in Figure 2E. Here, according to the stoichiometric ratio, each Te (2) nanorod carries only 69 magnetite nanoparticles, much less than the Te (1) nanorod in Figure 2C due to its smaller size and less surface, although both are under their own critical concentration of the nanoparticles, respectively. In order to illustrate the hydrophobic interaction between the oleic acid capped nanoparticles and P*t*BMA polymer protected Te nanorods, a single Te (2) magnetic nanorod carrying *ca.* 50 nanoparticles is enlarged in Figure 2F, where the spacing between the nanoparticles and Te nanorod is clearly visible. Here, the strong hydrophobic interaction fixes and "suspends" the nanoparticles in the dense polymer matrix on the nanorod surface.

Characterization of Magnetic Nanocylinders. To detail the assembly of magnetite nanoparticles, the formed magnetic Te (1) nanocylinders at the critical concentration of nanoparticles are subjected to further investigations. Figure 3A displays a TEM image of a single magnetic Te (1) nanocylinder. An enlarged view of its end (the inset in Figure 3A) reveals a dense layer of nanoparticles on the nanorod surface. At several sites on the nanorod (indicated by black arrows), packing with double layers of nanoparticles is also detected. The electron diffraction pattern of the single magnetic nanocylinder is displayed in Figure 3B. As expected, both dotted and ring-shaped patterns appear simultaneously. The dotted pattern represents the single-crystalline Te nanorod, as the "backbone" of the nanocylinder, and the ring-shaped pattern for the randomly oriented nanoparticles on the nanorod. In fact, the whole pattern resembles a simple overlap of the diffraction patterns of magnetite nanoparticles (Figure 1D) and a single Te nanorod (Figure 1I).

The morphological change of the Te nanorods before and after covering with nanoparticles can be easily observed in their scanning electron microscopy (SEM) images. In Figure 3C, the pure Te nanorods exhibit a rigid and homogeneous surface. The mean diameter is 50.9 ± 6.6 nm, 4 nm wider than that from TEM analysis, since the P*t*BMA layer on the nanorods is visible in SEM. The decoration with magnetite nanoparticles roughens the smooth surface of the nanorods, as shown in Figure 3D. Instead of a flat surface, bright dots

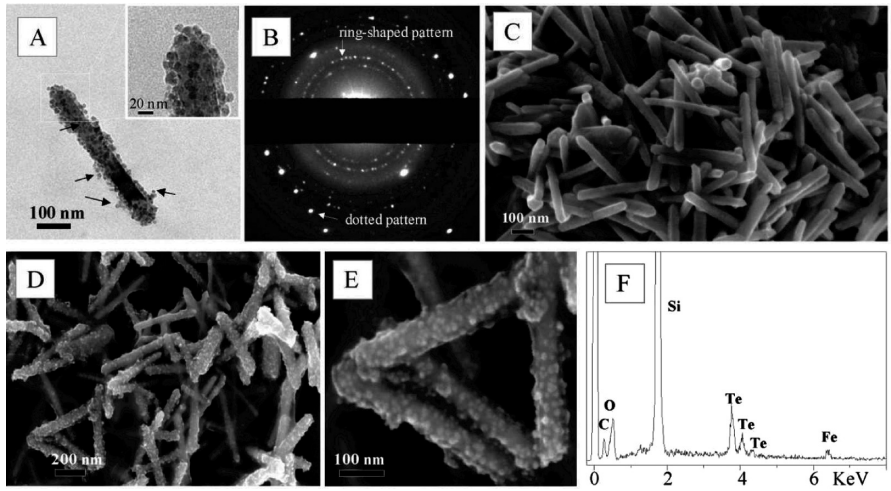

Figure 3. Electron microscopy analysis of the magnetic Te (1) nanocylinders prepared by Te (1) nanorods (60 mg/L) and magnetite nanoparticles at the critical concentration (5.2 mg/L). (A) TEM image of a single magnetic nanocylinder; (B) its electron diffraction pattern; (C) the SEM image of the pure Te nanorods; (D) SEM image of the magnetic nanocylinders; (E) its enlarged view; and (F) the corresponding elemental analysis.

appear all over the nanorods. The enlarged view is shown in Figure 3E. Differently from the TEM analysis of the individual magnetic nanocylinders, the SEM image offers direct evidence on how nanoparticles pack on the nanorod surface. It is found that, although congested with the bright dots (the oleic acid capped magnetite nanoparticles), some space of the nanorod surface remains unoccupied by nanoparticles. Free space between the nanoparticles is frequently observed, and a monolayer close-packing does not exist. This is in accordance with a theoretical calculation, where we found that each nanorod (1) could hold 660 magnetite nanoparticles on its surface by monolayer close-packing (see Supporting Information), much more than the observed 167 nanoparticles. We believe that the sites on the nanorods, which were occupied by P*t*BMA polymers, introduce a spatial repulsion and eventually prevent magnetite nanoparticles on the nanorod surface from packing closely with each other. Figure 3F is the result obtained from the energy-dispersive X-ray (EDX) analysis of the magnetic nanocylinders. Only the signals of carbon, oxygen, iron, and Te are detected (Si signal from the substrate). They are the exact constructing elements of the oleic acid capped magnetite nanoparticles and the P*t*BMA attached Te nanorods. Despite of the rough baseline, we still calculate a weight ratio of 1:8.1 (12%) for Fe_3O_4/Te, which is close to the theoretical value, 1:11 (9%).

Magnetic Nanocylinders with Overloaded Magnetite Nanoparticles. Our further effort was aimed to exceed the limitation of loading magnetite nanoparticles onto the nanorods. Here, a concentration of magnetite nanoparticles of 300 mg/L, well above the critical concentration (5.2 mg/L), was used to form the magnetic Te (1) nanocylinders. The excessive nanoparticles were removed by sonication and then ultrafiltration using a PTFE membrane with a pore size of 200 nm. The TEM images of the magnetic Te (1) nanocylinders before and after purification are shown in Figure 4. In Figure 4A, the nanoparticles, although enriched on the Te nanorods, spread all over the space. The loosely attached nanoparticles were first dissociated from the nanocylinders by sonication and then filtered away by

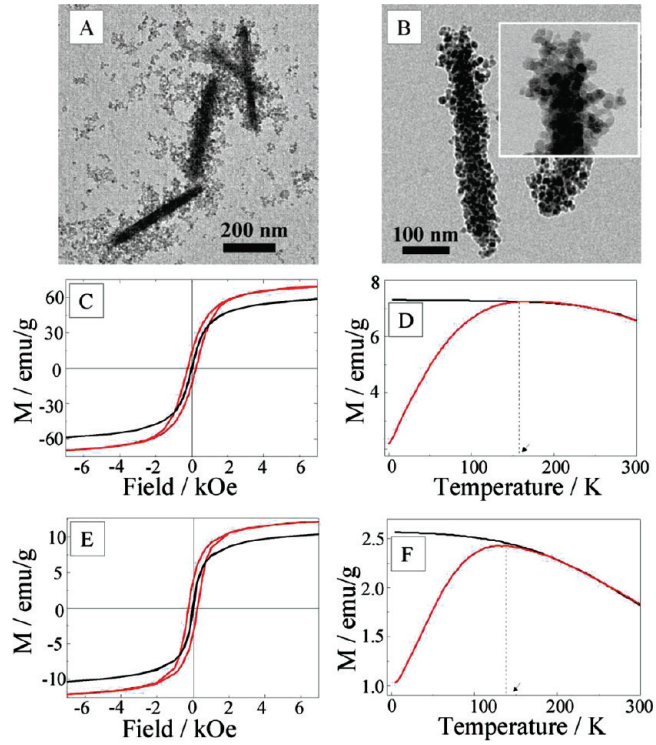

Figure 4. (A,B) TEM images of magnetic Te (1) nanocylinders formed with 300 mg/L of magnetite nanoparticles and 60 mg/L of Te (1) nanorods before and after purification (sonication and ultrafiltration); (C) magnetization curves *M*(*H*) for the magnetite nanoparticles at 300 K (black line) and 5 K (red line); (D) ZFC (red line) and FC (black line) curves with the temperature ranging from 5 to 300 K; (E) magnetization curves *M*(*H*) for the magnetic nanocylinders at 300 K (black line) and 5 K (red line); and (F) ZFC (red line) and FC (black line) curves of the magnetic nanocylinders with the temperature ranging from 5 to 300 K.

ultrafiltration. Figure 4B shows an individual purified magnetic nanocylinder, where more nanoparticles were evidently found on the nanorod than that formed at the critical concentration (Figure 3A). Due to the oversaturation with the nanoparticles on the surface, the contour shape of the nanorod can hardly be distinguished. The nanorod is completely covered with almost two layers of nanoparticles. Its structure was further investigated at a high magnification on its top, as shown in the inset in Figure 4B. It is easy to see that the nanoparticles even pile up on some sites of nanorod surface to form protrusions. The overloading enables a high content of magnetite nanoparticles in the nanocylinders.

To estimate the amount of the magnetite nanoparticles in such overloaded nanocylinders, superconducting quantum interference device (SQUID) measurements were performed for both the magnetite nanoparticles and the purified magnetic nanocylinders. Figure 4C presents the hysteresis curves $M(H)$ of the nanoparticles at 300 and 5 K. The magnetite nanoparticles are superparamagnetic at 300 K and ferromagnetic at 5 K, which is typical for magnetite nanoparticles.[64,65] The remanence, coercivity, and saturation magnetization at 5 K are 13.3 emu/g, 229 Oe, and 69 emu/g, respectively. The blocking temperature is determined as 160 K from the zero field cooling (ZFC) and field cooling (FC) curves in Figure 4D. In the case of magnetic nanocylinders, whose magnetic properties are exclusively arising from the magnetite nanoparticles, the shape of the $M(H)$ curve is rather similar to that of the magnetite nanoparticles. At 5 K, the coercivity is 259 Oe, very close to that of the pure nanoparticles since the physical properties (size, crystallinity, capping agent, *etc.*) of the spherical and isotropic nanoparticles were maintained during the assembly process. The only significant difference lies in the remanence and saturation magnetization, which are 13.3 and 69 emu/g for nanoparticles but only 3.7 and 12 emu/g for nanocylinders at 5 K. Such difference is commonly caused by the volume-dilution effect of magnetite nanoparticles in the formed nanocylinder structure. According to the saturation magnetization of the nanoparticles before and after assembly on Te nanorods, 15 wt % of magnetite nanoparticles on the nanocylinders is calculated,[66] which is almost twice as high as the 8 wt % calculated from the nanocylinders formed at the critical concentration. The blocking temperature of the magnetic nanocylinders slightly shifted to 140 K in Figure 4F, 20 K lower than the pure magnetite nanoparticles. The small difference could come from the assembly process. We assume that, in the presence of excessive nanoparticles, small ones are easier to be inserted into the P*t*BMA polymer matrix on the nanorod surface than the large ones. Thus, the nanoparticles that have been assembled on the nanorods contain a larger fraction of small nanoparticles, which decreases the average size of the assembled magnetite nanoparticles. As reported, the change in the size of the magnetic nanoparticles is reflected in the blocking temperature.[67−69] It is worth noting that the magnetic nanocylinders based on the immobilization of magnetite nanoparticles on the Te nanorods remain superparamagnetic at room temperature, whereas single-phase magnetite nanorods with the same size (422 nm long, 47 nm wide) would exhibit ferromagnetic behavior because of the transition of superparamagnetism to ferromagnetism for magnetite nanoparticles above ~25 nm at room temperature.[70,71] In the field of magnetorheology, superparamagnetic nanorods are of great interest because, after the removal of external magnetic field, they do not retain any magnetism (coercivity), which avoids additional magnetic forces among nanorods and the corresponding agglomeration in solution.

Alignment of the Magnetic Nanocylinders in an External Magnetic Field. The magnetic Te (2) nanocylinders shown in Figure 2E were further checked with respect to their response to a magnetic field. It was first visualized by responding to an external magnet, as shown in Figure 5A−C. The responsive behavior of the magnetic nanocylinders in solution to the magnetic field can be utilized to align the nanocylinders on a solid substrate. To prepare the sample, the magnetic nanocylinder solution was dropped on a carbon-coated copper TEM grid fixed on the tip of a plastic sample holder, which was immediately inserted into a magnetic field of 0.3 T parallel to the TEM grid surface. Figure 5D shows the aligned magnetic nanocylinders on the TEM grid. Due to the magnetic nanoparticles on the surface, the longitudinal axis of all Te nanorods is almost parallel to the magnetic field, quite different from the randomly oriented Te nanorods. A similar ordering of 1-D magnetic nanostructures (nickel or nickel-based alloy nanowires) in an external magnetic field has also been reported.[30,31] The structure of the nanocylinders shows high stability in the strong magnetic field; only very few magnetite nanoparticles were dissociated from the nanocylinders during the alignment, as shown in Figure 5D.

Very interestingly, a linear connection of the nanocylinders was often found in the TEM images. Figure 5E presents an example of this elongated superstructure, which is made up of five individual magnetic nanocylinders *via* end-to-end junction. This behavior resembles that of macroscopic magnetic rods, which are connected at the ends *via* magnetic dipolar interaction. The whole linear superstructure points to the same direction as the magnetic field. These ordered superstructures were not observed in the absence of the external magnetic field in our studies. To detail how the nanocylinders are connected at both ends, two junctions were enlarged in Figure 5F,G. In Figure 5F, the two nanocylinders are combined by a small joint at both ends, but the two faces of the ends are nearly mismatched. Differently in Figure 5G, the two

nanocylinders are parallel to each other and connected directly face-to-face at both ends despite of a rather small translation perpendicular to the longitudinal axis of the nanorods.

Demagnetization of Prealigned Magnetic Nanocylinders. The oriented nanocylinders, whose magnetic properties originate from the magnetite nanoparticles, can be readily demagnetized by a selective etching process in an aqueous acid solution, namely, dissolving the magnetite nanoparticles from the nanorods. Very significantly, the etching will keep the Te nanorods in an aligned state, as the hydrophobic polymer shell on the nanorod in the aqueous solution acts as a cage, fixing and "freezing" the nanorods on the substrate. Figure 6A−D shows the original and stepwise HCl-etched magnetic nanocylinders after 20, 40, and 60 min, which present a clear trend of decreasing population and size of nanoparticles on the nanorod. Unexpectedly, a few magnetite particles were still observed anchoring the nanorod surface after 60 min etching (indicted by the white circle in Figure 6D). The unusual stability of magnetite nanoparticles against strong HCl acid (pH = 1) is owed to the hydrophobic alkyl chains of oleic acid on the nanoparticle surface that are further immobilized in the hydrophobic polymer matrix on the nanorod. In such intensive hydrophobic environment, the diffusion of HCl molecules to the magnetite nanoparticles is retarded.

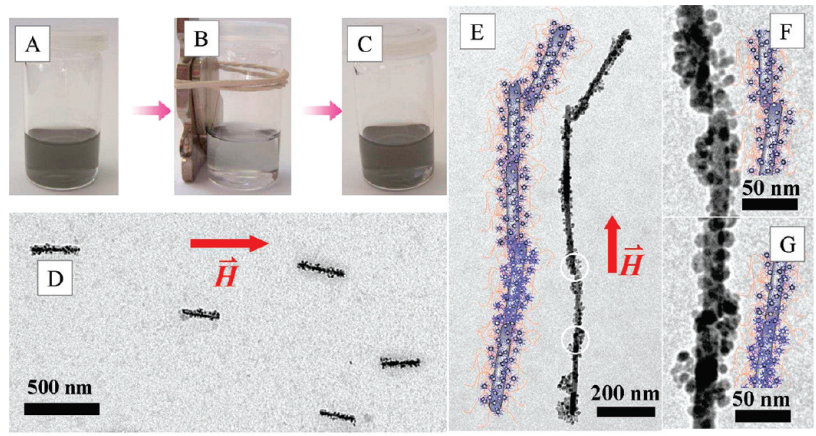

Figure 5. (A) Magnetic Te (2) nanocylinder solution in THF; (B) when close to a magnet; (C) after leaving the magnet and shaking; (D) TEM image of aligned magnetic nanocylinders when deposited from solution onto a carbon-coated TEM grid in the presence of an external magnetic field (0.3 T); (E) linear connection of aligned magnetic nanocylinders. The cartoon on the left side illustrates how this linear superstructure has been constructed. (F,G) Enlarged views of the junctions of the magnetic nanocylinders indicated by the white circles in panel E.

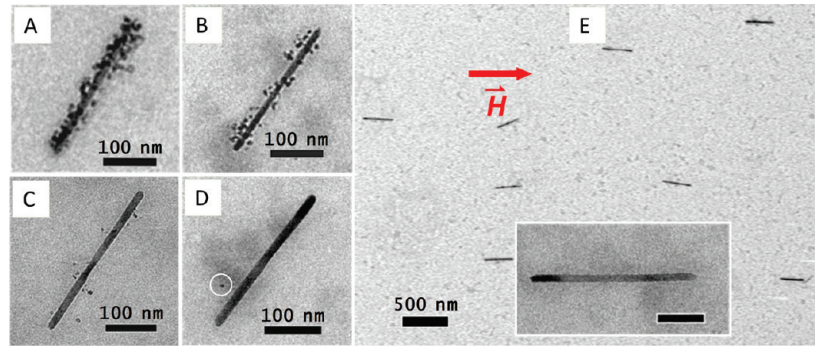

Figure 6. (A−D) TEM images of the original Te (2) magnetic nanocylinders, and the stepwise HCl-etched ones after 20, 40, and 60 min; (E) Te (2) nanorods after the complete etching of nanoparticles (80 min) from the nanorod surface. The inset in panel E is an enlarged view of a single rod.

The etching process was accomplished after 80 min. Figure 6E shows a representative TEM image of the aligned Te nanorods after etching away the nanoparticles (more images in Figure s4, Supporting Information). The longitudinal axis of these nanorods points to the same direction as the external magnetic field. In the enlarged view (inset in Figure 6E) of a single nanorod, the nanorod surface is clearly flat and free of nanoparticles, indicating the successful demagnetization of the Te nanorod. It should be mentioned that, although hydrochloric acid is not able to attack Te,[72] some nanorods were spotted becoming thinner specifically in the center during the etching process (Figures 6C,D and s4 in Supporting Information) due to the rather vigorous corrosiveness of HCl. The covering density of the aligned nanorods in our approach is, however, limited by the nanocylinder concentration. At a higher concentration, the long polymer chains tethered to the nanorod surface can entangle with each other, which interferes with the nanorod orientation when drying in a magnetic field. Nevertheless, the coverage can be improved in practice by repeating the deposition−drying process in the same substrate area to enrich the nanorods.

The methodology of decorating nanorods with magnetite nanoparticles, aligning and etching of the formed magnetic nanocylinders (MAD process), can be broadened as a general method to align nonmagnetic 1-D nanostructures assisted by an external magnetic field. The type of 1-D nanostructures, polymer layers, magnetic nanoparticles, and surfactants can be specially combined and designed for a specific application. For example, the polymeric layer on the nanostructures can be created either during the formation of the 1-D nanostructures, like in our case, or more commonly *via* surface-initiated polymerization techniques[73,74] and "grafting onto" methods.[75]

CONCLUSIONS

In conclusion, we have successfully aligned Te nanorods *via* an interesting magnetization−alignment−demagnetization (MAD) process assisted by an external magnetic field. The assembly of magnetite nanoparticles onto Te nanorods in THF solution can be quantitatively controlled in terms of their stoichiometric ratio below a

critical concentration of the nanoparticles. Due to the polymer and surfactant on their surface, the formed magnetic nanocylinders are soluble in THF, which enables the alignment of these nanocylinders on a solid substrate in the presence of an external magnetic field. By an acid-etching process, they were demagnetized into Te nanorods in an organized manner. This MAD process can be extended as a general procedure for the alignment of nonmagnetic 1-D nanostructures. Additionally, the magnetic nanocylinders based on the Te nanorods and magnetite nanoparticles can be potentially applied in the field of magnetorheology, where the ordering of magnetic nanocylinders by an external field may record the signals or change the fluid viscosity.

METHODS

Preparation of Linear Poly(*tert*-butyl methacrylate) (P*t*BMA). P*t*BMA with high molecular weight was synthesized by atom transfer radical polymerization (ATRP). Briefly, 0.049 g (0.5 mmol) of CuCl catalyst with 0.086 g (0.5 mmol) of *N*,*N*,*N*′,*N*′′,*N*′′-pentamethyldiethylenetriamine in 10 mL of toluene, 0.095 g (0.5 mmol) of the initiator *p*-toluenesulfonyl chloride in 4 mL of toluene, and 42.66 g (0.3 mol) of purified *t*BMA in 40 mL of toluene were first prepared and bubbled with argon for 10 min in three separated screw cap glasses. After transferring the catalyst and initiator to *t*BMA monomer with a nitrogen-flashed syringe, the solution was stirred in an oil bath at 90 °C for 26 h. Then the mixture was cooled to room temperature and filtered through an Al_2O_3 column. After precipitation in water/methanol, the product was freeze-dried from dioxane. The number-averaged molecular weight is 95 000 g/mol, and the polydispersity is 1.09, measured from a conventional GPC using THF as eluent and P*t*BMA as standard.

Preparation of Magnetite Nanoparticles. The oleic acid capped magnetite nanoparticles were prepared by the co-precipitation method.[34,35] Briefly, 28.1 g of $FeCl_3 \cdot 6H_2O$ in 550 mL of water and 10.9 g of $FeCl_2 \cdot 4H_2O$ in 30 mL of H_2O (with 4 drops of fuming HCl) were mixed and kept at 60 °C. A black precipitate appeared when 90 mL of aqueous NH_4OH (25%) was added to the solution. After stirring for 10 min, the black precipitate was separated by magnet and washed with H_2O until pH 9. To cap the surface with oleic acid, the mixture of 300 mL of water and 32 mL of 10 wt % oleic acid in paraffin oil was added. After heating at 80 °C for 1 h, the oleic acid capped nanoparticles were separated by magnet, and the black oil phase was washed with water and ethanol to remove the excess oleic acid. Further filtration through glass fiber was carried out to remove any agglomerates, and the mixture was centrifuged for 1 h (4000 rms, 30 °C).

Preparation of Te Nanorods. The Te nanorods were prepared from the room-temperature decomposition of H_2Te gas in a P*t*BMA solution in THF.[15] As an example, the synthesis of Te (1) nanorods was carried out under a gentle argon flow at room temperature. A three-necked flask with magnetic stirrer, with 1.25 g of aluminum telluride (Al_2Te_3, 99.5% pure, Gerac), and 60 mL of dioxane, was equipped with a bubble counter and connected to a pipeline inserted into a 250 mL reaction flask containing 200 mL of P*t*BMA solution (0.5 g/L) in THF. The dispersion of Al_2Te_3 in dioxane and the P*t*BMA solution in THF were bubbled with argon for 30 min. Then 10 mL of oxygen-free H_2SO_4 solution (0.5 M) was added dropwise by a syringe pump within 2 h. The generated H_2Te gas was distributed *via* argon flow into the reaction flask. At the end, argon was further bubbled for 30 min, and the reaction flask was further stirred overnight. For the synthesis of Te (2) nanorods, 2 g of Al_2Te_3 and 1 g/L of P*t*BMA in THF were used; in the case of Te (3) nanorods, 1.6 g of Al_2Te_3 and 0.5 g/L of P*t*BMA in THF were used.

Preparation and Alignment of Magnetic Nanocylinders. The assembly of magnetite nanoparticles on the Te nanorod surface was achieved by adding different amounts of magnetite nanoparticle solution into the Te nanorod solution in THF under strong mechanical shaking under argon for 2 h. The magnetic nanocylinders were aligned in a magnetic field of 0.3 T. The sample was prepared by placing one drop of the magnetic nanocylinder solution in THF on a carbon-coated TEM grid and immediately inserted into the magnetic field, which was parallel to the TEM grid surface.

Demagnetization Process. The acid-etching process was carried out in an aqueous HCl solution (pH = 1) under an argon atmosphere to avoid the oxidation of the Te nanorods. The aligned magnetic nanocylinders on a carbon-coated copper TEM grid were immersed into the aqueous HCl solution for a desired period. To monitor the etching process, the sample was taken out after 20, 40, 60, and 80 min and rinsed by pure water before subjected to the TEM investigation.

Transmission Electron Microscopy (TEM). TEM images and the electron diffraction patterns were taken on a Zeiss EM EF-TEM instrument operated at 200 kV. For each sample, a 2 μL droplet of the solution was deposited onto a carbon-coated copper TEM grid.

Scanning Electron Microscopy (SEM). SEM was performed using a Zeiss 1530 Gemini instrument equipped with a field emission cathode with a lateral resolution of approximately 2 nm. The sample was prepared by placing one drop of the solution onto a purified silicon wafer.

Superconducting Quantum Interference Device (SQUID) Measurement. Magnetic properties of the samples were studied with a Quantum Design MPMS-XL superconducting quantum interference device magnetometer between 300 and 5 K, with a maximum applied field of 50 kOe (=5 T). The magnetization was also measured as a function of temperature at a given applied field in the field cooled (FC) and zero field cooled (ZFC) modes. For the ZFC measurements, the sample was first cooled down to 5 K in zero magnetic field. Subsequently, a magnetic field of 100 Oe (10 mT) was applied and the magnetization was measured while the temperature was increased up to 300 K. Afterward, the magnetization of the sample under a magnetic field of 100 Oe as a function of decreasing temperature (down to 5 K) was measured as the FC magnetization.

Size Distribution Analysis. The statistical analysis of the size distribution of the nanoparticles and nanorods was performed using the UTHSCSA ImageTool program (University of Texas). In each sample, 100 ± 10 objects were measured to define the dimension.

Acknowledgment. This work was financially supported by the Deutsche Forschungsgemeinschaft (SPP1165, Grant Mu896/22). We thank Benjamin Gossler for the kind help in SEM measurements. The authors would like to thank Verena Jung and Dr. Vadim Ksenofontov for the Mössbauer measurements and discussions.

Supporting Information Available: Mössbauer spectrum of the magnetite nanoparticles, details of Te (2) and Te (3) nanorods and their assembly with magnetite nanoparticles, calculation of the population of magnetite nanoparticles per Te nanorod according to their concentrations in THF, calculation of the population of nanoparticles per Te nanorod by monolayer close-packing from their dimension, Te nanorods in an aligned state *via* the "MAD" process. This material is available free of charge *via* the Internet at http://pubs.acs.org.

REFERENCES AND NOTES

1. Xia, Y.; Yang, P.; Sun, Y.; Wu, Y.; Mayers, B.; Gates, B.; Yin, Y.; Kim, F.; Yan, H. One-Dimensional Nanostructures: Synthesis, Characterization, and Applications. *Adv. Mater.* **2003**, *15*, 353–389.
2. Wang, X.; Song, J.; Liu, J.; Wang, Z. L. Direct-Current Nanogenerator Driven by Ultrasonic Waves. *Science* **2007**, *316*, 102–105.
3. Dai, H.; Hafner, J. H.; Rinzler, A. G.; Colbert, D. T.; Smalley, R. E. Nanotubes as Nanoprobes in Scanning Probe Microscopy. *Nature* **1996**, *384*, 147–150.
4. Jain, P. K.; Eustis, S.; El-Sayed, M. A. Plasmon Coupling in Nanorod Assemblies: Optical Absorption, Discrete Dipole

Approximation Simulation, and Exciton-Coupling Model. *J. Phys. Chem. B* **2006**, *110*, 18243–18253.
5. Murphy, C. J.; Sau, T. K.; Gole, A. M.; Orendorff, C. J.; Gao, J.; Gou, L.; Hunyadi, S. E.; Li, T. Anisotropic Metal Nanoparticles: Synthesis, Assembly, and Optical Applications. *J. Phys. Chem. B* **2005**, *109*, 13857–13870.
6. Hu, J.; Li, L.; Yang, W.; Manna, L.; Wang, L.; Alivisatos, A. P. Linearly Polarized Emission from Colloidal Semiconductor Quantum Rods. *Science* **2001**, *292*, 2060–2063.
7. Huynh Wendy, U.; Dittmer Janke, J.; Alivisatos, A. P. Hybrid Nanorod-Polymer Solar Cells. *Science* **2002**, *295*, 2425–2427.
8. Sudeep, P. K.; Joseph, S. T. S.; Thomas, K. G. Selective Detection of Cysteine and Glutathione Using Gold Nanorods. *J. Am. Chem. Soc.* **2005**, *127*, 6516–6517.
9. Huang, X.; El-Sayed, I. H.; Qian, W.; El-Sayed, M. A. Cancer Cell Imaging and Photothermal Therapy in the Near-Infrared Region by Using Gold Nanorods. *J. Am. Chem. Soc.* **2006**, *128*, 2115–2120.
10. Gorelikov, I.; Field, L. M.; Kumacheva, E. Hybrid Microgels Photoresponsive in the Near-Infrared Spectral Range. *J. Am. Chem. Soc.* **2004**, *126*, 15938–15939.
11. Salem Aliasger, K.; Searson Peter, C.; Leong Kam, W. Multifunctional Nanorods for Gene Delivery. *Nat. Mater.* **2003**, *2*, 668–671.
12. Duan, X.; Lieber, C. M. General Synthesis of Compound Semiconductor Nanowires. *Adv. Mater.* **2000**, *12*, 298–302.
13. Ma, C.; Wang, Z. L. Road Map for the Controlled Synthesis of CdSe Nanowires, Nanobelts, and Nanosaws—A Step towards Nanomanufacturing. *Adv. Mater.* **2005**, *17*, 2635–2639.
14. Grebinski, J. W.; Richter, K. L.; Zhang, J.; Kosel, T. H.; Kuno, M. Synthesis and Characterization of Au/Bi Core/Shell Nanocrystals: A Precursor toward II−VI Nanowires. *J. Phys. Chem. B* **2004**, *108*, 9745–9751.
15. Adelung, R.; Aktas, O. C.; Franc, J.; Biswas, A.; Kunz, R.; Elbahri, M.; Kanzow, J.; Schuermann, U.; Faupel, F. Strain-Controlled Growth of Nanowires within Thin-Film Cracks. *Nat. Mater.* **2004**, *3*, 375–379.
16. Milenkovic, S.; Hassel Achim, W.; Schneider, A. Effect of the Growth Conditions on the Spatial Features of Re Nanowires Produced by Directional Solidification. *Nano Lett.* **2006**, *6*, 794–799.
17. Yuan, J.; Xu, Y.; Walther, A.; Bolisetty, S.; Schumacher, M.; Schmalz, H.; Ballauff, M.; Müller, A. H. E. Water-Soluble Organo-Silica Hybrid Nanowires. *Nat. Mater.* **2008**, *7*, 718–722.
18. Li, L.-s.; Walda, J.; Manna, L.; Alivisatos, A. P. Semiconductor Nanorod Liquid Crystals. *Nano Lett.* **2002**, *2*, 557–560.
19. Zhu, Y. F.; Chen, M.; Wei, Z.; Zhang, R. P.; Nikhil, K.; Ji, L. Alignment of Multiwalled Carbon Nanotubes in Bulk Epoxy Composites *via* Electric Field. *J. Appl. Phys.* **2009**, *105*, 054319.
20. Thomas, K. G.; Barazzouk, S.; Ipe, B. I.; Joseph, S. T. S.; Kamat, P. V. Uniaxial Plasmon Coupling through Longitudinal Self-Assembly of Gold Nanorods. *J. Phys. Chem. B* **2004**, *108*, 13066–13068.
21. Joseph, S. T. S.; Ipe, B. I.; Pramod, P.; Thomas, K. G. Gold Nanorods to Nanochains: Mechanistic Investigations on Their Longitudinal Assembly Using α,ω-Alkanedithiols and Interplasmon Coupling. *J. Phys. Chem. B* **2006**, *110*, 150–157.
22. Nie, Z.; Fava, D.; Kumacheva, E.; Zou, S.; Walker, G. C.; Rubinstein, M. Self-Assembly of Metal-Polymer Analogues of Amphiphilic Triblock Copolymers. *Nat. Mater.* **2007**, *6*, 609–614.
23. Khanal, B. P.; Zubarev, E. R. Rings of Nanorods. *Angew. Chem., Int. Ed.* **2007**, *46*, 2195–2198.
24. Caswell, K. K.; Wilson, J. N.; Bunz, U. H. F.; Murphy, C. J. Preferential End-to-End Assembly of Gold Nanorods by Biotin-Streptavidin Connectors. *J. Am. Chem. Soc.* **2003**, *125*, 13914–13915.
25. Dujardin, E.; Mann, S.; Hsin, L.-B.; Wang, C. R. C. DNA-Driven Self-Assembly of Gold Nanorods. *Chem. Commun.* **2001**, *14*, 1264–1265.
26. Zhang, Q.; Gupta, S.; Emrick, T.; Russell, T. P. Surface-Functionalized CdSe Nanorods for Assembly in Diblock Copolymer Templates. *J. Am. Chem. Soc.* **2006**, *128*, 3898–3899.
27. Correa-Duarte, M. A.; Perez-Juste, J.; Sanchez-Iglesias, A.; Giersig, M.; Liz-Marzan, L. M. Aligning Au Nanorods by Using Carbon Nanotubes as Templates. *Angew. Chem., Int. Ed.* **2005**, *44*, 4375–4378.
28. Gupta, S.; Zhang, Q.; Emrick, T.; Russell, T. P. "Self-Corralling" Nanorods under an Applied Electric Field. *Nano Lett.* **2006**, *6*, 2066–2069.
29. Ryan, K. M.; Mastroianni, A.; Stancil, K. A.; Liu, H.; Alivisatos, A. P. Electric-Field-Assisted Assembly of Perpendicularly Oriented Nanorod Superlattices. *Nano Lett.* **2006**, *6*, 1479–1482.
30. Hangarter, C. M.; Rheem, Y.; Yoo, B.; Yang, E.-H.; Myung, N. V. Hierarchical Magnetic Assembly of Nanowires. *Nanotechnology* **2007**, *18*, 205305.
31. Hangarter, C. M.; Myung, N. V. Magnetic Alignment of Nanowires. *Chem. Mater.* **2005**, *17*, 1320–1324.
32. Park, S.; Lim, J.-H.; Chung, S.-W.; Mirkin, C. A. Self-Assembly of Mesoscopic Metal-Polymer Amphiphiles. *Science* **2004**, *303*, 348–351.
33. Huang, X.; Li, L.; Luo, X.; Zhu, X.; Li, G. Orientation-Controlled Synthesis and Ferromagnetism of Single Crystalline Co Nanowire Arrays. *J. Phys. Chem. C* **2008**, *112*, 1468–1472.
34. Huang, Y.; Duan, X.; Wei, Q.; Lieber, C. M. Directed Assembly of One-Dimensional Nanostructures into Functional Networks. *Science* **2001**, *291*, 630–633.
35. Kim, F.; Kwan, S.; Akana, J.; Yang, P. Langmuir−Blodgett Nanorod Assembly. *J. Am. Chem. Soc.* **2001**, *123*, 4360–4361.
36. Islam, M. F.; Alsayed, A. M.; Dogic, Z.; Zhang, J.; Lubensky, T. C.; Yodh, A. G. Nematic Nanotube Gels. *Phys. Rev. Lett.* **2004**, *92*, 088303.
37. Lagerwall, J.; Scalia, G.; Haluska, M.; Dettlaff-Weglikowska, U.; Roth, S.; Giesselmann, F. Nanotube Alignment Using Lyotropic Liquid Crystals. *Adv. Mater.* **2007**, *19*, 359–364.
38. Ghezelbash, A.; Koo, B.; Korgel, B. A. Self-Assembled Stripe Patterns of CdS Nanorods. *Nano Lett.* **2006**, *6*, 1832–1836.
39. Li, Y.; Wu, Y. Coassembly of Graphene Oxide and Nanowires for Large-Area Nanowire Alignment. *J. Am. Chem. Soc.* **2009**, *131*, 5851–5857.
40. Wang, X.; Liu, Y.; Yu, G.; Xu, C.; Zhang, J.; Zhu, D. Anisotropic Electrical Transport Properties of Aligned Carbon Nanotube Films. *J. Phys. Chem. B* **2001**, *105*, 9422–9425.
41. Peter, A. S.; Christopher, D. N.; Thomas, N. J.; Theresa, S. M.; Benjamin, R. M.; Jeremiah, M.; Thomas, E. M. Electric-Field Assisted Assembly and Alignment of Metallic Nanowires. *Appl. Phys. Lett.* **2000**, *77*, 1399–1401.
42. Salem, A. K.; Chao, J.; Leong, K. W.; Searson, P. C. Receptor-Mediated Self-Assembly of Multi-Component Magnetic Nanowires. *Adv. Mater.* **2004**, *16*, 268–271.
43. Tanase, M.; Bauer, L. A.; Hultgren, A.; Silevitch, D. M.; Sun, L.; Reich, D. H.; Searson, P. C.; Meyer, G. J. Magnetic Alignment of Fluorescent Nanowires. *Nano Lett.* **2001**, *1*, 155–158.
44. Kordas, K.; Mustonen, T.; Toth, G.; Vahakangas, J.; Jantunen, H.; Gupta, A.; Rao, K. V.; Vajtai, R.; Ajayan, P. M. Magnetic-Field Induced Efficient Alignment of Carbon Nanotubes in Aqueous Solutions. *Chem. Mater.* **2007**, *19*, 787–791.
45. Shi, D.; He, P.; Lian, J.; Xavier, C.; Sergey, L. B. k.; Eric, B.; Wang, L. M.; Rodney, C. E.; Robert, T. Magnetic Alignment of Carbon Nanofibers in Polymer Composites and Anisotropy of Mechanical Properties. *J. Appl. Phys.* **2005**, *97*, 064312.
46. Lee, S.-W.; Jeong, M.-C.; Myoung, J.-M.; Chae, G.-S.; Chung, I.-J. Magnetic Alignment of ZnO Nanowires for Optoelectronic Device Applications. *Appl. Phys. Lett.* **2007**, *90*, 133115.

47. Bentley, A. K.; Trethewey, J. S.; Ellis, A. B.; Crone, W. C. Magnetic Manipulation of Copper−Tin Nanowires Capped with Nickel Ends. *Nano Lett.* **2004**, *4*, 487–490.
48. Ooi, C.; Yellen, B. B. Field Gradients Can Control the Alignment of Nanorods. *Langmuir* **2008**, *24*, 8514–8521.
49. Chinchun, O.; Randall, M. E.; Benjamin, B. Y. On the Controllability of Nanorod Alignment in Magnetic Fluids. *J. Appl. Phys.* **2008**, *103*, 07E910.
50. Yuan, J.; Schmalz, H.; Xu, Y.; Miyajima, N.; Drechsler, M.; Möller, M. W.; Schacher, F.; Müller, A. H. E. Room-Temperature Growth of Uniform Tellurium Nanorods and the Assembly of Tellurium or Fe_3O_4 Nanoparticles on the Nanorods. *Adv. Mater.* **2008**, *20*, 947–952.
51. Lu, A. H.; Salabas, E. L.; Schüth, F. Magnetic Nanoparticles: Synthesis, Protection, Functionalization, and Application. *Angew. Chem., Int. Ed.* **2007**, *46*, 1222–1244.
52. Zhang, M.; Estournes, C.; Bietsch, W.; Müller, A. H. E. Superparamagnetic Hybrid Nanocylinders. *Adv. Funct. Mater.* **2004**, *14*, 871–882.
53. Gao, J.; Zhang, B.; Zhang, X.; Xu, B. Magnetic-Dipolar-Interaction-Induced Self-Assembly Affords Wires of Hollow Nanocrystals of Cobalt Selenide. *Angew. Chem., Int. Ed.* **2006**, *45*, 1220–1223.
54. Huang, Z.; Zhang, Y.; Tang, F. Solution-Phase Synthesis of Single-Crystalline Magnetic Nanowires with High Aspect Ratio and Uniformity. *Chem. Commun.* **2005**, 342–344.
55. Hu, X.; Yu, J. C. High-Yield Synthesis of Nickel and Nickel Phosphide Nanowires *via* Microwave-Assisted Processes. *Chem. Mater.* **2008**, *20*, 6743–6749.
56. Sellmyer, D. J.; Zheng, M.; Skomski, R. Magnetism of Fe, Co and Ni Nanowires in Self-Assembled Arrays. *J. Phys.: Condens. Matter* **2001**, *13*, R433–R460.
57. Fert, A.; Piraux, L. Magnetic Nanowires. *J. Magn. Magn. Mater.* **1999**, *200*, 338–358.
58. Gole, A.; Stone, J. W.; Gemmill, W. R.; zur Loye, H.-C.; Murphy, C. J. Iron Oxide Coated Gold Nanorods: Synthesis, Characterization, and Magnetic Manipulation. *Langmuir* **2008**, *24*, 6232–6237.
59. Yang, S.; Liu, H. A Novel Approach to Hollow Superparamagnetic Magnetite/Polystyrene Nanocomposite Microspheres *via* Interfacial Polymerization. *J. Mater. Chem.* **2006**, *16*, 4480–4487.
60. Kang, Y. S.; Risbud, S.; Rabolt, J. F.; Stroeve, P. Synthesis and Characterization of Nanometer-Size Fe_3O_4 and γ-Fe_2O_3 Particles. *Chem. Mater.* **1996**, *8*, 2209–2211.
61. Lee, H. S.; Lee, W. C.; Furubayashi, T. A Comparison of Coprecipitation with Microemulsion Methods in the Preparation of Magnetite. *J. Appl. Phys.* **1999**, *85*, 5231–5233.
62. Gee, S. H.; Hong, Y. K.; Erickson, D. W.; Park, M. H.; Sur, J. C. Synthesis and Aging Effect of Spherical Magnetite (Fe_3O_4) Nanoparticles for Biosensor Applications. *J. Appl. Phys.* **2003**, *93*, 7560–7562.
63. Li, J.; Tang, S.; Lu, L.; Zeng, H. C. Preparation of Nanocomposites of Metals, Metal Oxides, and Carbon Nanotubes *via* Self-Assembly. *J. Am. Chem. Soc.* **2007**, *129*, 9401–9409.
64. Woo, K.; Hong, J.; Choi, S.; Lee, H. W.; Ahn, J. P.; Kim, C. S.; Lee, S. W. Easy Synthesis and Magnetic Properties of Iron Oxide Nanoparticles. *Chem. Mater.* **2004**, *16*, 2814–2818.
65. Lee, D. K.; Kang, Y. S.; Lee, C. S.; Stroeve, P. Structure and Characterization of Nanocomposite Langmuir−Blodgett Films of Poly(maleic monoester)/Fe_3O_4 Nanoparticle Complexes. *J. Phys. Chem. B* **2002**, *106*, 7267–7271.
66. Galindo-Gonzalez, C.; De Vicente, J.; Ramos-Tejada, M. M.; Lopez-Lopez, M. T.; Gonzalez-Caballero, F.; Duran, J. D. G. Preparation and Sedimentation Behavior in Magnetic Fields of Magnetite-Covered Clay Particles. *Langmuir* **2005**, *21*, 4410–4419.
67. Bodker, F.; Morup, S. Size Dependence of the Properties of Hematite Nanoparticles. *Europhys. Lett.* **2000**, *52*, 217–223.
68. Hanson, M.; Johansson, C.; Pedersen, M. S.; Morup, S. The Influence of Particle Size and Interactions on the Magnetization and Susceptibility of Nanometer-Size Particles. *J. Phys.: Condens. Matter* **1995**, *7*, 9269–9277.
69. Thakur, M.; De, K.; Giri, S.; Si, S.; Kotal, A.; Mandal, T. K. Interparticle Interaction and Size Effect in Polymer Coated Magnetite Nanoparticles. *J. Phys.: Condens. Matter* **2006**, *18*, 9093–9104.
70. Liu, X.; Kaminski, M. D.; Guan, Y.; Chen, H.; Liu, H.; Rosengart, A. J. Preparation and Characterization of Hydrophobic Superparamagnetic Magnetite Gel. *J. Magn. Magn. Mater.* **2006**, *306*, 248–253.
71. Yang, T.-I.; Brown, R. N. C.; Kempel, L. C.; Kofinas, P. Magneto-Dielectric Properties of Polymer-Fe_3O_4 Nanocomposites. *J. Magn. Magn. Mater.* **2008**, *320*, 2714–2720.
72. Budavari, S.; O'Neil, M.; Smith, A.; Heckelman, P. *The Merck Index*, 11th ed.; Merck & Co: Rahway, NJ, 1989; p 9026.
73. Tang, C.; Bombalski, L.; Kruk, M.; Jaroniec, M.; Matyjaszewski, K.; Kowalewski, T. Nanoporous Carbon Films from "Hairy" Polyacrylonitrile-Grafted Colloidal Silica Nanoparticles. *Adv. Mater.* **2008**, *20*, 1516–1522.
74. Duan, H.; Kuang, M.; Wang, D.; Kurth Dirk, G.; Mohwald, H. Colloidally Stable Amphibious Nanocrystals Derived from Poly{[2-(dimethylamino)ethyl] methacrylate} Capping. *Angew. Chem., Int. Ed.* **2005**, *44*, 1717–1720.
75. Tahir, M. N.; Zink, N.; Eberhardt, M.; Therese, H. A.; Faiss, S.; Janshoff, A.; Kolb, U.; Theato, P.; Tremel, W. Hierarchical Assembly of TiO_2 Nanoparticles on WS_2 Nanotubes Achieved through Multifunctional Polymeric Ligands. *Small* **2007**, *3*, 829–834.